29 August 1997

ELSEVIER

Chemical Physics Letters 275 (1997) 188–198

CHEMICAL PHYSICS LETTERS

On the origin of spinning sidebands in MQMAS NMR experiments

Laura Marinelli, Lucio Frydman

Department of Chemistry (M / C 111), University of Illinois at Chicago, 845 W. Taylor Street, Chicago, IL 60607-7061, USA

Received 17 March 1997; in final form 15 May 1997

Abstract

We have recently demonstrated that a combination of multiple-quantum NMR and magic-angle spinning can provide high resolution spectra from half-integer quadrupolar nuclei. An interesting feature of these spectra is the appearance of extensive spinning sideband patterns along the indirectly detected dimension, whose origin is here discussed. It is shown that these sidebands arise even in the absence of explicit time modulations of any spin interactions, due to the orientation- and time-dependence characterizing the multiple- to single-quantum conversion process. An analytical formalism is developed to describe these effects, and corroborated by numerical calculations and NMR experiments. © 1997 Elsevier Science B.V.

1. Introduction

The enhancement of spectral resolution has always constituted a central goal in solid state nuclear magnetic resonance (NMR). These efforts were rewarded long ago in the case of dilute spin-1/2 spectroscopy with the introduction of magic-angle spinning (MAS) and dipolar decoupling, techniques which enable the routine acquisition of high resolution ^{13}C, ^{15}N or ^{31}P NMR spectra [1–3]. The purpose of MAS in these experiments is to modulate chemical shift interactions around their isotropic value, thus collapsing what were originally broad powder patterns into sharp solution-like centerbands [4]. Very often this fast spinning regime where the rate of rotation exceeds the size of all anisotropies cannot be mechanically achieved, thus leading to spectra where isotropic centerbands appear flanked by sideband peaks separated from one another by multiples of the rotor spinning speed [4,5]. More challenging than the dilute spin-1/2 case has been the achievement of high resolution for the case of half-integer nuclei with spin numbers larger than 1/2 ($S = 3/2, 5/2, 7/2, 9/2$), as here coherent averaging also has to deal with the anisotropies generated by the coupling between nuclear quadrupole moments and their surrounding electric field gradients. Furthermore although both chemical shift and quadrupolar interactions are described by second rank tensors the large size of the latter also demands the removal of its second order effects, anisotropies that are not susceptible to a MAS-type averaging regardless of the spinning angle chosen [6,7].

This long-standing problem in the NMR spectroscopy of solids was resolved in the late eighties by means of

PII S0009-2614(97)00746-X

a novel formalism which, by focusing on the central transition of the nuclear spin manifold and making the axis of sample spinning time dependent, enabled the simultaneous removal of all first and second order spectral anisotropies [8,9]. Two new experiments crystallized as a result of these considerations: double rotation (DOR), a 1D NMR version where samples are spun about two axes simultaneously [10], and dynamic angle spinning (DAS), a 2D version where the two spinning angles are adopted consecutively [11]. In spite of the importance that these new methods have both from a conceptual as well as from an applied stand point, their routine use as analytical tools has been limited as a result of certain technical and fundamental complications. An experiment capable of bypassing these limitations was recently introduced based on an alternative approach, whereby the axis of sample spinning is kept constant at the magic angle but the transition order defining the spin evolution is made time dependent [12]. The resulting 2D multiple-quantum (MQ) MAS experiment can then achieve a refocusing of all spin anisotropies that is analogous to the one occurring in DAS, albeit involving conventional NMR hardware. Experimental considerations restrict the order of the directly detected spin evolution to the $-1/2 \leftrightarrow +1/2$ central transition, and although the indirect spin evolution can be selected at will from among the reminder $-m \leftrightarrow +m$ multiquantum transitions in the spin manifold, signal-to-noise (S/N) considerations usually make the triple-quantum $-3/2 \leftrightarrow +3/2$ transition the preferred choice [13]. The resulting triple-/single-quantum 2D correlation experiment provides a considerable resolution enhancement over conventional MAS acquisitions, and in the two years that have elapsed since its introduction numerous demonstrations of its potential have appeared in the literature.

Fig. 1 illustrates the kind of spectra that this technique provides using the single ^{23}Na resonance of the model compound Na_2SO_4 as a test example. These data were acquired by means of a two-pulse sequence [14–17], and processed using a shearing transformation that enables the retrieval of a high resolution trace [14]. Besides an enhanced site resolution this spectrum exhibits an unusual feature along the indirectly detected domain, involving potentially intense spinning sidebands that are largely absent along the central transition ν_2 axis. These sidebands have actually been noted in the majority of MQMAS studies reported in the literature, and are known to deteriorate the overall spectral S/N and preclude accurate numerical analyses of the resolved powder line shapes [19]. Explaining the origin of these sidebands and predicting their relative intensities are the main concerns of the present report.

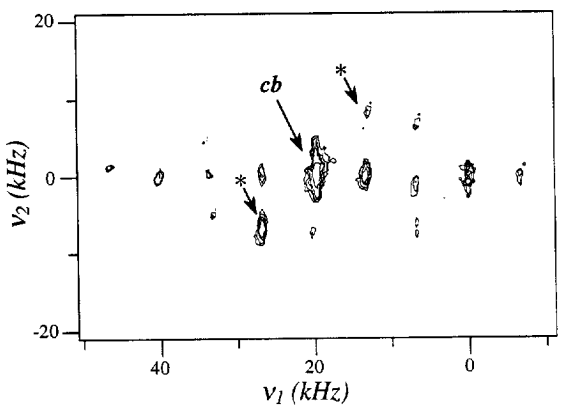

Fig. 1. ^{23}Na MQMAS NMR spectrum of Na_2SO_4 recorded at 4.7 T with sample spinning at $\omega_r/2\pi = 6$ kHz. Data were acquired using a two-pulse sequence ($\omega_1/2\pi \approx 100$ kHz) and processed as described elsewhere [14]. Contours are shown spaced between 4 and 40% of the maximum centerband (*cb*) intensity; asterisks indicate spinning sidebands originating from modulations of the central transition anisotropies which are shifted along ν_1 as a result of a shearing of the data [18]. All remaining spinning sidebands, appearing mainly along the indirectly detected ν_1 axis, constitute the focus of the present investigation.

Like their more conventional central transition MAS counterparts, multiple-quantum MAS sidebands are spaced at multiples of the rotor frequency and decrease in intensity as the spinning speed is increased. Unlike the former, however, their considerable intensities seem to extend beyond the static line width of the unidimensional powder pattern. A possible explanation for this behavior could lie in the magnified chemical shift and dipolar effects that are known to affect the evolution of multiple-quantum coherences in comparison to central single-quantum $-1/2 \leftrightarrow +1/2$ transitions. Quantitative considerations, however, reveal that neither of these factors provides a reasonable explanation for the strong ν_1 spinning sidebands appearing in Fig. 1. Dipolar effects in this sample are relatively weak and are fully averaged out by the MAS process, otherwise their homogeneous nature would prevent the retrieval of sharp MQMAS signals. Alkali metals like ^{23}Na also exhibit a very modest range of shielding anisotropies, at most a few 10's of ppm [20], and these values are in frequency units much smaller than the spinning speed involved. Another potential source for the ν_1 sidebands could reside in the modulation of anisotropic second order quadrupole effects. Numerical simulations reveal, however, that this mechanism constitutes again an unviable explanation for the ν_1 sidebands, as the second order MAS sideband patterns originated by triple-quantum coherences are much weaker than those originated by modulations of their central single-quantum counterparts (Fig. 2). These arguments indicate that the unequal intensities that spinning sidebands exhibit along the two dimensions of an MQMAS spectrum cannot be explained by traditional models involving the rotational modulation of spin interactions. The next Section introduces an alternative analysis that clarifies this situation by providing a physical explanation for the origin of these spinning sidebands, as well as a quantitative description of their intensities in terms of the relevant spectral parameters. The predictions of this analytical formalism are subsequently validated by numerical simulations and by comparisons with experimental data collected under different conditions.

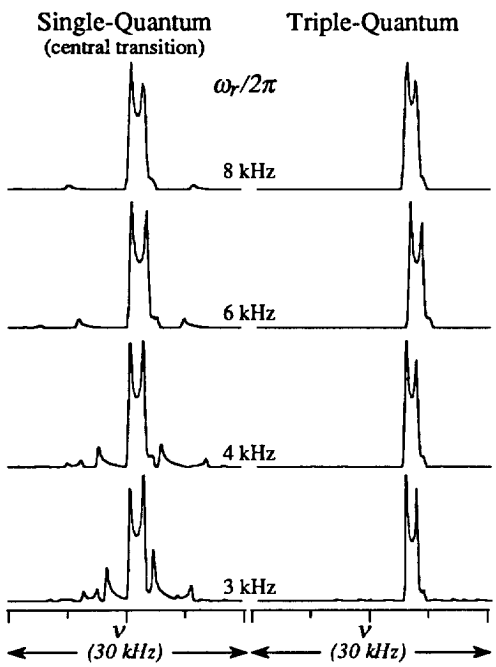

Fig. 2. Variable spinning speed simulations of idealized single- and triple-quantum MAS line shapes arising from a spin-3/2 powder in the presence of second order quadrupole effects. The parameters employed in these calculations correspond to an on-resonance ^{23}Na site at 4.7 T with a coupling constant $e^2qQ/h = 2.6$ MHz and an asymmetry parameter $\eta = 0$.

2. The origin of MQMAS sidebands

In order to identify the physical origin of the intense ν_1 spinning sidebands appearing in MQMAS spectra we begin by considering a simple but relevant type of situation involving a single-site spin-3/2 powder affected by couplings to dominant Zeeman and perturbing radiofrequency (rf) magnetic fields, as well as by a first order quadrupole interaction. On this system we consider the application of a two-pulse 2D MQMAS sequence

$$(\tau_1)_{\phi_1} - t_1 - (\tau_2)_{\phi_2} - t_2(\phi_{Rx}), \tag{1}$$

where τ_1, τ_2 denote the durations of the triple-quantum excitation and conversion pulses (a few μs long [13,14]), ϕ_1, ϕ_2 are the relative rotating frame phases of these pulses, t_1, t_2 are the evolution and acquisition periods corresponding to the propagation of triple- and single-quantum coherences, and all ϕ_i phases are cycled so as to select the appropriate MQMAS coherence transfer pathways. A simplified time dependence will also be assumed for the rotating frame Hamiltonian $\mathscr{H}(t)$ acting on the spins during the course of this experiment, given (in angular frequency units) by

$$\mathscr{H}(t) = \begin{cases} \omega_Q(\tau_1)\cdot\left[3S_z^2 - S(S+1)\right] + \omega_1 S_x & 0 \le t < \tau_1, \quad \text{(excitation)} \\ \omega_Q(t)\cdot\left[3S_z^2 - S(S+1)\right] & \tau_1 \le t < \tau_1 + t_1, \quad \text{(evolution)} \\ \omega_Q(\tau_1 + t_1 + \tau_2)\cdot\left[3S_z^2 - S(S+1)\right] + \omega_1 S_x & \tau_1 + t_1 \le t < \tau_1 + t_1 + \tau_2, \quad \text{(conversion)} \\ \omega_Q(t)\cdot\left[3S_z^2 - S(S+1)\right] & \tau_1 + t_1\tau_2 \le t. \quad \text{(acquisition)} \end{cases} \tag{2}$$

In this equation S, $\{S_i\}_{i=x,z}$ denote the usual spin operators, ω_1 is the nutation rate imposed by the applied rf pulses, and

$$\omega_Q(t) = \frac{2\pi(e^2qQ/h)}{4S(2S-1)}\left[A_1\cos(\omega_r t + \gamma) + A_2\sin(\omega_r t + \gamma) + B_1\cos(2\omega_r t + 2\gamma) + B_2\sin(2\omega_r t + 2\gamma)\right] \tag{3}$$

is the first order quadrupolar frequency of a particular crystallite [21]. The instantaneous value of this interaction depends on the coupling constant e^2qQ/h, on the asymmetry parameter η, on the sample spinning rate ω_r, and on Euler angles $\Omega = (\alpha, \beta, \gamma)$ defining the relative orientation of the quadrupolar tensor with respect to a reference frame fixed on the sample spinner. The full expressions for the angular coefficients in Eq. (3) are

$$A_1 = \frac{\sqrt{2}\sin\beta\cos\beta(\eta\cos2\alpha - 3)}{3}, \quad A_2 = -\frac{\sqrt{2}\,\eta\sin\beta\sin2\alpha}{3},$$

$$B_1 = \frac{3/2\cdot\sin^2\beta + 1/2\cdot\eta\cos2\alpha(1+\cos^2\beta)}{3}, \quad B_2 = -\frac{\eta\cos\beta\sin2\alpha}{3}. \tag{4}$$

The Hamiltonian in Eq. (2) neglects any explicit modulation of the sample spinning on the quadrupole interaction during the duration of the rf pulses. Although this assumption is justified by the short duration of the pulses in comparison to a typical rotor period, τ_1, $\tau_2 \approx 0.05\cdot(2\pi/\omega_r)$, its consideration is not critical and an explicit propagation of $\mathscr{H}(t)$ during the rf pulses can still be carried out by integrating its effects over the excitation and conversion times. More relevant is the explicit omission in Eq. (2) of second order quadrupole, shielding and dipolar anisotropies, since by leaving these terms out we are ensuring that neither triple- nor single-quantum spin evolutions will undergo any explicit time oscillations during t_1 or t_2. In spite of the absence of these time dependent interactions, the Hamiltonian in Eq. (2) still predicts the appearance of

potentially intense spinning sidebands along the indirect ν_1 dimension. This can be demonstrated by computing the total powder signal S arising from the experiment

$$S(t_1,t_2) = \int_{\Omega} \mathrm{Tr}\left[S_+^{2-3} \cdot \rho(\tau_1 + t_1 + \tau_2 + t_2)\right] \mathrm{d}\Omega, \tag{5}$$

in terms of the final spin density matrix $\rho(\tau_1 + t_1 + \tau_2 + t_2)$. An analytical expression for this state can be calculated as

$$\rho(\tau_1 + t_1 + \tau_2 + t_2) = a \cdot U(\tau_1 + t_1 + \tau_2 + t_2) \cdot S_z \cdot U^{-1}(\tau_1 + t_1 + \tau_2 + t_2), \tag{6}$$

where $a = h\nu_L/kT$ is a Curie factor scaling the initial S_z equilibrium matrix and U denotes the total time evolution operator of the experiment:

$$U(\tau_1 + t_1 + \tau_2 + t_2) = \exp\left[-\mathrm{i}\int_{t_2} \mathscr{H}(t)\mathrm{d}t\right] \cdot \exp\left[-\mathrm{i}\mathscr{H}(t = \tau_1 + t_1 + \tau_2) \cdot \tau_2\right] \cdot \exp\left[-\mathrm{i}\int_{t_1} \mathscr{H}(t)\mathrm{d}t\right] \cdot \exp\left[-\mathrm{i}\mathscr{H}(t = \tau_1) \cdot \tau_1\right]. \tag{7}$$

The integrated expressions in this equation correspond to phases acquired during the t_1 and t_2 free evolution periods, whereas the remaining exponentials correspond to forced nutations occurring during the excitation and conversion pulses. Phase cycling can be artificially introduced in this time propagation by preserving during t_1 only those off-diagonal elements associated to triple-quantum coherences, and during t_2 only the central transition magnetization elements.

Although the t_1 and t_2 integrals in Eq. (7) are effectively zero due to the inability of $\mathscr{H}(t)$ to modulate either

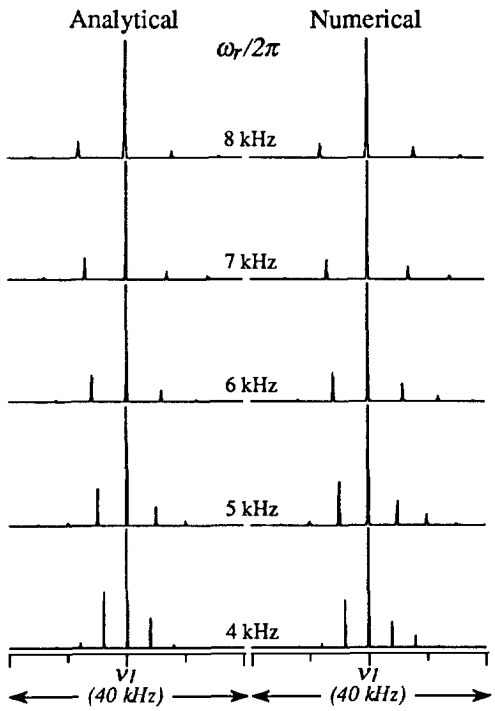

Fig. 3. Comparison between the ν_1 variable spinning speed spectra predicted by the analytical theory in Section 2 (left-hand column), and simulations obtained by Fourier transforming time domain signals calculated from a numerical propagation of the spin Hamiltonian. Both sets of simulations considered a spin-3/2 powder free from shielding and second order effects. A first order quadrupolar interaction with $e^2qQ/h = 3$ MHz, $\eta = 0$, and rf pulses $\omega_1 \cdot \tau_1 = 2\pi \cdot 0.8$ cycles, $\omega_1 \cdot \tau_2 = 2\pi \cdot 0.2$ cycles, $\omega_1/2\pi = 100$ kHz were assumed in the calculations.

triple- or single-quantum coherences, $S(t_1, t_2)$ still exhibits a t_1 dependence that arises due to the different eigenvalues adopted by $\mathscr{H}$ at times $t = \tau_1$ and $t = \tau_1 + t_1 + \tau_2$. Indeed, in between these two pulses the quadrupole tensor of each crystallite will undergo a rotor-driven reorientation, which imposes on the rf nutation angles a time modulation that is periodic modulo $2\pi/\omega_r$. A simple expression for these nutation phases can be retrieved by expanding the Hamiltonian's eigenvalues as a function of ω_1/ω_Q, and exploiting the fact that since ω_Q is generally much larger than ω_1 only terms up to powers of $(\omega_1/\omega_Q)^2$ need to be considered [22–24]. The final expression of the time domain signal then takes the form

$$S(t_1,t_2) = 3a\sin(\omega_1\tau_2)\cdot\int_{\Omega}\sin\left[\phi_{13}^{(1)}(\Omega)\right]\cdot\left\{\tfrac{3}{2}\exp\left[i\phi_{14}^{(2)}(\Omega)\right] + \exp\left[i\phi_{23}^{(2)}(\Omega)\right]\right\}d\Omega, \tag{8}$$

where

$$\phi_{13}^{(1)}(\Omega) = \frac{3}{8}\left[\frac{\omega_1}{\omega_Q(\tau_1)}\right]^2\omega_1\cdot\tau_1 \tag{9}$$

are the orientation-dependent nutation angles acquired by triple-quantum coherences during their excitation, and

$$\underset{23}{\phi_{14}^{(2)}}(\Omega) = \pm 2\int_{\tau_1}^{\tau_1+t_1+\tau_2}\omega_Q(t)dt \tag{10}$$

are t_1-dependent nutation phases describing the conversion of multiple-quantum coherences into single-quantum signals.

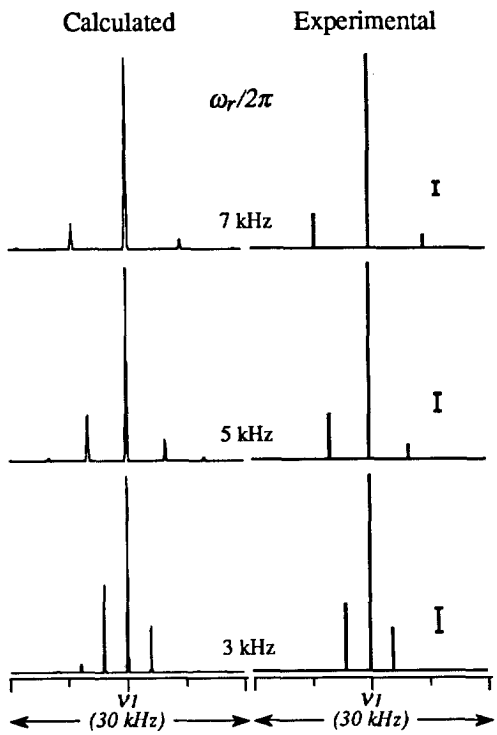

Fig. 4. Comparison between the ν_1 spinning sideband intensities predicted by the analytical theory described in Section 2 (left-hand column), and ^{23}Na MQMAS NMR results observed in variable speed experiments on $Na_2C_2O_4$ at 4.7 T. The experimental stick plots were obtained by integrating the volumes of all ν_2 powder patterns in the 2D spectrum associated to each ν_1 spinning sideband; notice that the former are shifted with respect to one another as a result of the shearing (Fig. 1, Ref. [18]). Brackets on the right of each experimental spectrum describe the error intervals of these integration procedures, as judged by repetitive measurements. Simulations employed literature $Na_2C_2O_4$ quadrupolar coupling constants [25], as well as the spinning and irradiation parameters associated with each experiment.

The t_1 dependence involved in Eq. (10) and its role in the $S(t_1, t_2)$ signal provides a mechanism for the generation of ν_1 spinning sidebands that does not involve the explicit oscillation of any spin interaction. Furthermore this t_1 dependence appears modulating a first order quadrupole effect, and is thus likely to result in sideband patterns extending over a far wider range than those of its central transition counterpart. The quantification of the ν_1 sidebands predicted by this phenomenon can be simplified by replacing the lower and upper limits of the integral in Eq. (10) by 0 and t_1 respectively, an approximation that is again justified by the $\tau_1, \tau_2 \ll (2\pi/\omega_r)$, t_1 condition. This results in multiple-quantum conversion phases of the form

$$\begin{aligned}\phi^{(2)}_{\substack{14\\23}}(t_1) &= \pm\left[\frac{2\pi e^2 qQ/h}{2S(2S-1)}\right]\cdot\left\{\frac{A_1}{\omega_r}\left[\sin(\omega_r t_1+\gamma)-\sin\gamma\right]-\frac{A_2}{\omega_r}\left[\cos(\omega_r t_1+\gamma)-\cos\gamma\right]\right.\\ &\left.+\frac{B_1}{2\omega_r}\left[\sin(2\omega_r t_1+2\gamma)-\sin(2\gamma)\right]-\frac{B_2}{2\omega_r t}\left[\cos(2\omega_r t_1+2\gamma)-\cos(2\gamma)\right]\right\}\\ &= \pm\left\{A'_1\left[\sin(\omega_r t_1+\gamma)-\sin\gamma\right]-A'_2\left[\cos(\omega_r t_1+\gamma)-\cos\gamma\right]\right.\\ &\left.+B'_1\left[\sin(2\omega_r t_1+2\gamma)-\sin(2\gamma)\right]-B'_2\left[\cos(2\omega_r t_1+2\gamma)-\cos(2\gamma)\right]\right\},\end{aligned} \tag{11}$$

which contain the typical $\omega_r t$-, $2\omega_r t$-dependence that originates spinning sidebands in spin-1/2 NMR experiments [4]. The positions and intensities of the resulting peaks can be calculated by substituting these expressions for $\phi^{(2)}_{14}$, $\phi^{(2)}_{23}$ nto Eq. (8), and then carrying out a Bessel analysis of the powder signal based on the relation

$$e^{iz\sin\phi}=\sum_{k=-\infty}^{\infty}J_k(z)e^{ik\phi}. \tag{12}$$

The total time domain signal can then be expressed as

$$S(t_1,t_2)=\sum_{N=-\infty}^{\infty}\left[\tfrac{3}{2}I_N e^{iN\omega_r t_1}+I_{-N}e^{-iN\omega_r t_1}\right], \tag{13}$$

where the integrals $I_{\pm N}$

$$I_{\pm N}=3a\sin(\omega_1\tau_2)\int_{\Omega}\left\{\sin\phi^{(1)}_{13}(\Omega)\right\}\cdot F_{\pm N}(\Omega)\,d\Omega \tag{14}$$

determine the intensities of the Nth order sidebands via the Bessel coefficients $F_{\pm N}$:

$$\begin{aligned}F_N(\Omega)=2\pi&\sum_{k=-\infty}^{\infty}J_k(A'_1)\sum_{k'=-\infty}^{\infty}J_{k'}(A'_1)\sum_{l=-\infty}^{\infty}J_l(A'_2)\sum_{l'=-\infty}^{\infty}J_{l'}(A'_2)\sum_{m=-\infty}^{\infty}J_m(B'_1)\sum_{m'=-\infty}^{\infty}J_{m'}(B'_1)\\ &\times\sum_{n=-\infty}^{\infty}J_n(A'_2)\sum_{n'=-\infty}^{\infty}J_{n'}(B'_2)\cdot\exp\left[i(l-l'+n-n')\pi/2\right],\end{aligned} \tag{15}$$

$$F_{-N}=(F_N)^*. \tag{16}$$

The arguments in these Bessel series are dependent on the $(e^2qQ/h)/\omega_r$ ratio and on η, and their sums need to be performed over all indices fulfilling

$$N=l-k+2(m-n),\quad N=l'-k'+2(m'-n'). \tag{17}$$

3. MQMAS sidebands: comparison with numerical calculations and experiments

The formalism described in the preceding Section has the important advantage of yielding in Eqs. (8)–(17) analytical expressions for the intensities of the MQMAS ν_1 sideband patterns. Prior to exploiting these

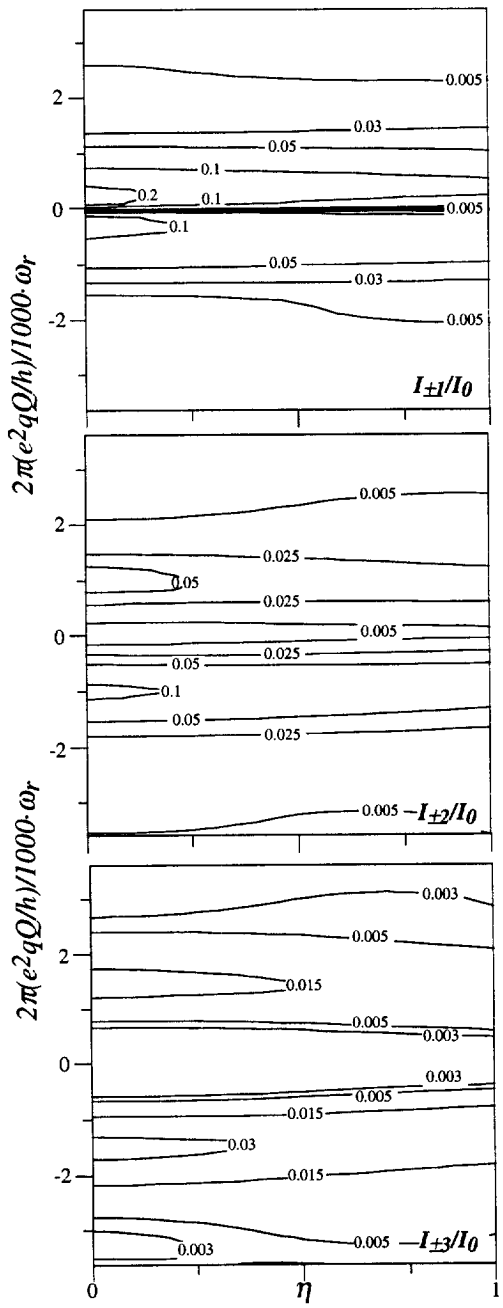

Fig. 5. Contour plots describing the relative intensities of Nth ν_1 spinning sidebands according to the analytical formalism outlined in Section 2, as a function of the parameters $2\pi(e^2qQ/h)/\omega_r$ and η under the assumption $\omega_1 \cdot \tau_1 = 2\pi \cdot 0.8$, $\omega_1 \cdot \tau_2 = 2\pi \cdot 0.2$ radians. Positive and negative values of $2\pi(e^2qQ/h)/\omega_r$ describe $+N$ and $-N$ sideband intensities respectively, thus making the absolute sense of sample rotation irrelevant.

expressions we decided to search for independent verifications supporting the assumptions that were involved in their derivations, and certifying that they do successfully describe the unusual sideband features observed in MQMAS acquisitions. These verifications were carried out by comparing the analytical predictions of the preceding Section with "brute force" numerical calculations of MQMAS spin evolutions under different conditions, as well as with results arising from variable spinning speed NMR experiments.

Fig. 3 compares for a set of typical experimental parameters and as a function of the $2\pi(e^2qQ/h)/\omega_r$ ratio, the ν_1 sideband spectra predicted by Eqs. (8)–(17) with those computed from an exact numerical time propagation of the spin system followed by Fourier transformation. The agreement between the sideband patterns calculated using the two different methods is very good, and this agreement holds not only for this particular set of spectral parameters but also for other representative situations including moderate chemical shift and second order quadrupole effects. Further corroboration on the usefulness of the model introduced in the preceding Section is presented in Fig. 4, where its predictions are compared with experimental ν_1 sideband intensities observed by ^{23}Na NMR for polycrystalline $Na_2C_2O_4$ as a function of the sample spinning rate. A good agreement between both sets is observed not only for moderate speeds but also for the slowest rates of sample rotation, for which spinning sidebands originating in the modulation of second order quadrupole effects are also present. This is another indication of the central role that the orientation- and t_1-dependences of the conversion process play in the generation of ν_1 MQMAS sidebands, a role that can be much more relevant than that played by other, more traditional sources of rotational modulation.

Once the quantitative capabilities of the theory described in the preceding Section have been verified, one can attempt to exploit the latter's analytical form in order to predict the general intensities that MQMAS sidebands in spin-3/2 experiments will exhibit in terms of the only two chemically relevant parameters involved: $2\pi(e^2qQ/h)/\omega_r$ and η. Unfortunately Eq. (14) also predicts that the total sideband intensities will vary upon changing the rf nutation angles $\omega_1 \cdot \tau_1$, $\omega_1 \cdot \tau_2$ used in the excitation and conversion of the triple-quantum coherence. In order to bypass this unwanted dependence and still derive a general description of the sideband intensities we decided to specify these angles of nutation to 0.8 and 0.2 cycles, values which have been shown to maximize the S/N of MQMAS experiments over a wide range of $(e^2qQ/h)/\omega_1$ conditions [13,14]. The analytical formalism could then be used to calculate for different spinning and quadrupolar parameters the ratio expected between the Nth sideband and the centerband intensities; results arising from these calculations are illustrated in Fig. 5. These plots are not expected to change drastically for minor adjustments in the durations of the pulses, and should consequently proof useful for the quantitative analysis of spinning sidebands in MQMAS spectra collected using the two-pulse sequence.

4. Discussion and conclusion

This work attempted to present a physical explanation for the unusual spinning sideband patterns observed in MQMAS NMR spectra along the indirect domain. After disregarding the modulation of shielding, dipolar and second order quadrupolar anisotropies as sources of the observed behavior, the origin of these sidebands was traced to the time- and orientation-dependences of the multiple-quantum conversion process. A similar non-traditional explanation for the origin of ν_1 sidebands was recently discussed by Spiess and co-workers in connection with double-quantum MAS NMR observations on coupled pairs of abundant nuclei [26,27]. Furthermore it is interesting to note that the mechanism originating ν_1 sidebands in these multiquantum experiments can be expected to be active in any 2D solid state NMR experiment, provided that it includes spinning of the sample and an orientation dependent mixing process between t_1 and t_2.

In order to quantify the ν_1 MQMAS sidebands in terms of the spectral parameters involved, we focused our analysis on the behavior expected when a two-pulse sequence is applied on spin-3/2 ensembles. Although limited in its scope this scenario covers a wide variety of chemically interesting systems, and further extensions to higher spin numbers [28,29] or to more complex pulse sequences are relatively straightforward. The effects of

chemical shielding or second order anisotropies can also be introduced in these analytical calculations with the aid of suitable perturbative expansions; results from these investigations will be reported in a future publication.

An important feature revealed by the present analysis is that MQMAS ν_1 sidebands will typically originate in modulations of first order quadrupole effects. The information encoded by the relative sideband intensities is thus controlled by e^2qQ/h and η, quadrupole parameters which can also become available in a simple fashion by analyzing the positions and line shapes of peaks in a 2D MQMAS spectrum [14]. This will probably deprive MQMAS spinning sidebands manifolds from much of the usefulness that characterized their spin-$1/2$ counterparts, whose spectra lacked a similar redundancy on their coupling information. The first order origin of MQMAS sidebands is also responsible for the considerably strong intensities of these rotor peaks, a feature which can potentially remove much of the centerband's signal even upon moderately fast spinning. A solution for this drawback has been recently proposed based on a sideband folding procedure achieved by incrementing the t_1 evolution in synchrony with the rotational period [19]. Now that the origin of MQMAS spinning sidebands has been clarified we trust that alternative sideband suppression schemes free from such sampling limitations will also begin to emerge.

Acknowledgements

We are grateful to Mr. Ales Medek for assistance in the collection of the experimental data. This work was supported by the National Science Foundation through grants DMR-9420458 and CHE-9502644 (CAREER Award); LF is a Beckman Young Investigator (1996–1998); Camille Dreyfus Teacher–Scholar (1996–2001); University of Illinois Junior Scholar (1997–2000); Alfred P. Sloan Fellow (1997–2000).

References

[1] E.R. Andrew, A. Bradbury, R.G. Eades, Nature 182 (1958) 1659.
[2] I.J. Lowe, Phys. Rev. Lett. 2 (1959) 285.
[3] J. Schaefer, E.O. Stejskal, J. Am. Chem. Soc. 98 (1976) 1031.
[4] M.M. Maricq, J.S. Waugh, J. Chem. Phys. 70 (1979) 3300.
[5] J. Herzfeld, A.E. Berger, J. Chem. Phys. 73 (1980) 6021.
[6] E. Kundla, A. Samoson, E. Lippmaa, Chem. Phys. Lett. 83 (1981) 229.
[7] S. Ganapathy, S. Schramm, E. Oldfield, J. Chem. Phys. 77 (1982) 4360.
[8] A. Llor, J. Virlet, Chem. Phys. Lett. 152 (1988) 248.
[9] E.W. Wooten, K.T. Muller, A. Pines, Acc. Chem. Res. 25 (1992) 209.
[10] A. Samoson, E. Lippmaa, A. Pines, Mol. Phys. 65 (1988) 1013.
[11] K.T. Mueller, B.Q. Sun, G.C. Chingas, J.W. Zwanziger, T. Terao, A. Pines, J. Magn. Reson. 86 (1990) 470.
[12] L. Frydman, J.S. Harwood, J. Am. Chem. Soc. 117 (1995) 5367.
[13] J.P. Amoureux, C. Fernandez, L. Frydman, Chem. Phys. Lett. 259 (1996) 347.
[14] A. Medek, J.S. Hardwood, L. Frydman, J. Am. Chem. Soc. 117 (1995) 12779.
[15] C. Fernandez, J.P. Amoureux, Chem. Phys. Lett. 242 (1995) 449.
[16] G. Wu, D. Rovnyak, B. Sun, R.G. Griffin, Chem. Phys. Lett. 249 (1996) 210.
[17] D. Massiot, B. Tonzo, D. Trumeau, J.P. Coutures, J. Virlet, P. Florian, P.J. Grandinetti, Solid State NMR 6 (1996) 73.
[18] P.J. Grandinetti, Y.K. Lee, J.H. Baltisberger, B.Q. Sun, A. Pines, J. Magn. Reson. A 102 (1993) 195.
[19] D. Massiot, J. Magn. Reson. A 122 (1996) 240.
[20] R.K. Harris and B.E. Mann, eds., NMR and the Periodic Table (Academic Press, New York, 1978).
[21] U. Haeberlen, High Resolution NMR in Solids, in: Advances in Mangetic Resonance, Suppl. 1, J.S. Waugh, ed. (Academic Press, New York, 1976).
[22] A. Wokaun, R.R. Ernst, J. Chem. Phys. 67 (1977) 1752.
[23] S. Vega, J. Chem. Phys. 68 (1978) 5518.
[24] R. Janssen and W.S. Veeman, J. Chem. Soc. Faraday Trans. 184 (1988) 3747.

[25] B.Q. Sun, Scalar Operators in Solid-State NMR, Ph.D. Dissertation, Materials Science Division, Lawrence Berkeley Laboratory and University of California, 1991.
[26] J. Gottwald, D.E. Demco, R. Graf, H.W. Spiess, Chem. Phys. Lett. 243 (1995) 314.
[27] H. Geen, J.J. Titman, J. Gottwald, H.W. Spiess, J. Magn. Reson. A 114 (1995) 264.
[28] P.P. Man, Mol. Phys. 78 (1993) 307.
[29] P.P. Man, P. Tougne, Mol. Phys. 83 (1994) 997.